Chemistry Publications   Chemistry Department

7-1-2021

Extending nanoscale patterning with multipolar surface plasmon resonances.

Issam Kherbouche

Danielle MacRae

Théo Geronimi Jourdain

François Lagugné-Labarthet

Azedine Lamouri

See next page for additional authors

Authors

Issam Kherbouche, Danielle MacRae, Théo Geronimi Jourdain, François Lagugné-Labarthet, Azedine Lamouri, Alexandre Chevillot Biraud, Claire Mangeney, and Nordin Félidj

Journal Name

ARTICLE TYPE

Extending nanoscale patterning with multipolar surface plasmon resonances†

Issam Kherbouche,[ab] D MacRae,[c] Théo Geronimi Jourdain,[a] F Lagugné-Labarthet,[c] Azedine Lamouri,[a] Alexandre Chevillot Biraud,[a] Claire Mangeney *[d] and Nordin Félidj *[a]

Plasmonic excitation of metallic nanoparticles can trigger chemical reactions at the nanoscale. Such optical effects can also be employed to selectively and locally graft photopolymer layers at the nanostructure surface, and, when combined with a surface functionalization agent, new pathways can be explored to modify the surface of a plasmonic nanoparticle. Among these approaches, diazonium salt chemistry is seen as an attractive strategy due to the high photoinduced reactivity of these salts. In this work, we demonstrate that it is possible to trigger the site-selective grafting of aryl films derived from diazonium salts on distinct nano-localized area of single gold nanotriangles, by taking advantage of their multipolar localized surface plasmon modes. It is shown the aryl film will preferentially graft in areas where the electric field enhancement is maximum, independently of the considered excited surface plasmon mode. These experimental findings are in very good qualitative agreement with the calculations of the local electric field, using the finite-difference time-domain (FDTD) method. We believe that this plasmonic-based approach will not only pave a new way for the spatially controlled surface functionalization of plasmonic nanoparticles, but also provide a general strategy to attach distinct molecules to hot spot regions on a single nanoparticle, opening promising prospects in sensing and multiplexing, and optically nano-scale patterning of functional groups.

a Université de Paris, ITODYS, CNRS, UMR 7086, 15 rue J-A de Baïf, F-75013 Paris, France; E-mail:nordin.felidj@univ-paris-diderot.fr

b UFR Biomedicale, UMR 8601 Université Paris Descartes Sorbonne Paris Cite, 45 Rue des Saint Pères, 70005 Paris, France

c Department of Chemistry, University of Western Ontario, 1151 Richmond St., London, Ontario N6A 5B7, Canada

d Université de Paris, Laboratoire de Chimie et Biochimie Pharmacologiques et Toxicologiques, LCBPT, UMR 8601 CNRS, F-75006 Paris, France; E-mail:claire.mangeney@parisdescartes.fr

† Electronic Supplementary Information (ESI) available: [details of any supplementary information available should be included here]. See DOI: 00.0000/00000000.

‡ Additional footnotes to the title and authors can be included *e.g.* 'Present address:' or 'These authors contributed equally to this work' as above using the symbols: ‡, §.

1 Introduction

Plasmonic nanoparticles with subwavelength size exhibit remarkable optical properties since they can support localized surface plasmon (LSP) resonances.[1] These LSP resonances are related to a collective oscillation of conduction electrons at the particle surface, the frequency of which depends on the size, the shape and the chemical composition of the particles, the inter-particle distance, and the refractive index of the surrounding medium.[2–4] LSP excitation results in an enhanced extinction in the far-field, mostly located in the visible and near-infrared spectral range for metals such as gold and silver, and a huge enhancement of the local electromagnetic field at the particle surface.[5–7] Therefore, plasmonic nanoparticles are particularly important for their high potential in non linear optics,[8] chemo-sensors[9,10] or substrates for surface-enhanced spectroscopies, such as surface-enhanced Raman scattering (SERS).[11,12]

In the last decade, it has been shown that metal nanoparticles can also act as reactive elements due to their ability to generate hot carriers, through plasmon decay.[13,14] When nanoparticles are in the vicinity of molecular compounds, hot electrons are extracted from the metal into available molecular orbitals of the adsorbates (*i.e.*, injection of electrons into an anti-bonding state), causing, for instance, the dissociation of a bond in the molecular adsorbate.[15–17] It has been shown that the transient ions can then react on the metal surface.[18] Through such plasmon-induced processes, many reactions have been controlled at the particle scale, such as the dissociation of H_2 or other photocatalytic reactions some of them being of societal importance such as water splitting and carbon dioxide reduction.[19,20] Interestingly, the mapping of the particle reactivity at the nanometer scale can be achieved, following precisely the spatial distribution of the electric field enhancement, under LSP excitation.[18,21]

In the context of plasmon-induced chemical surface functionalization, a major challenge exists in the ability to trigger the site-selective grafting of functional layers on distinct nanoscale areas around plasmonic nanostructures. Recently, we developed

an original route, based on aryl diazonium salt chemistry, to spatially control the surface functionalization of gold nanostructures under LSP excitation[22]. These molecules present the advantage to create strong covalent Au–C bonds with the surface, promoting stable interfacial links between the nanoparticles (NPs) and the organic functional layers[23]. In addition, they offer a wide range of terminal functional groups for future post-functionalization reactions[24,25]. The grafting mechanism relies on a two-step process involving *(i)* the reduction of diazonium salts yielding reactive aryl radicals able to attach covalently to the surface and *(ii)* the reaction of the aryl radicals on the already grafted layers[23]. The thickness of the polyaryl layers can thus be monitored from monolayers to multilayers up to a few tens of nanometers[26]. Using plasmon-driven reduction of aryl diazonium salts, it is possible to pattern the surface chemical properties of lithographic gold nanodisks with different types of functional polyaryl layers, through a change of the incident light polarization (from 0 to 90°)[26]. Interestingly, the grafting takes place specifically in the regions where the local field is enhanced[27,28].

Compared to isotropic shapes, triangular and pyramidal nanoparticles display even more intense electromagnetic fields due to their sharp corners[29–31]. In addition, their tunable optical properties as a function of the edge length can lead to various multipolar LSP modes at distinct wavelengths, with a high concentration of electromagnetic field at different locations of the triangular nanoparticles as well as the arrays composed of adjacent nanotriangles[31,32]. Therefore, such triangular-shaped particles could provide various spatially resolved grafting areas, via the excitation of distinct multipolar LSP modes[33].

To our knowledge, the excitation of diverse multipolar LSP modes in order to give access to a wide range of reactive nanoscale areas for the versatile site-selective surface functionalization of gold NPs has never been reported so far. In this work, we address this issue by considering regular arrays of gold triangular nanostructures with spectrally resolved in-plane multipolar LSP modes. Such structures, designed through electron beam lithography (EBL), display distinct intense bands in the visible and near infrared spectral range, depending on their lateral size[33]. Herein, we focused our attention on the first three lowest energy multipolar LSP modes, corresponding to the dipolar, quadrupolar and sextupolar LSP modes. These three modes are particularly interesting since they are characterized in the near-field by strong field enhancements located at distinct places, depending on the excited multipolar LSP mode. Plasmon-induced grafting of diazonium salts has proved to be very efficient in the case of salts bearing various functionalities such as carboxylic acid or hydroxyethyl, which can be easily post-functionalized, as already demonstrated in previous papers[26]. The diazonium salt which was used to induce the plasmon-mediated grafting of aryl films is 4- nitrobenzenediazonium tetrafluoroborate (4NBDT).[34] By taking advantage of the multipolar localized surface plasmon modes, we explored the possibility to expand the limits of surface chemistry by confining the grafted aryl layers in a wide variety of nanoscale regions of maximum electric field enhancement around the gold nanostructures, as schematized in the figure 1 (and displayed later in Figs. 3, 4,and 6). The experimental findings were compared to the calculations of the local electric field performed using the finite-difference time-domain (FDTD) method,[35] in order to reveal the close relationship between near-field enhancement and surface grafting. We believe that this plasmonic-based approach will not only pave an easy way for the functionalization of plasmonic nanoparticles, but also provide a general strategy to attach molecules to hot spot regions and further improve their SERS detection and analysis for (bio)sensing applications.[36]
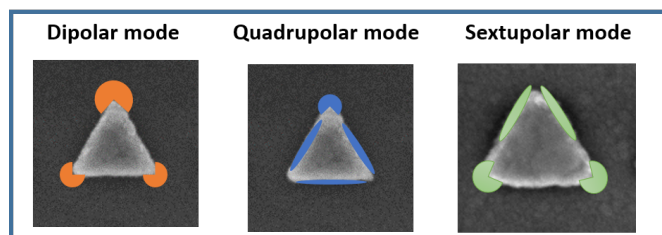

Fig. 1 Scheme of the strategy of multipolar plasmon-mediated surface functionalization. The location of the aryl film grafting will depend on the excited multipolar plasmon mode. It is expected that the grafting will take place specifically on the area sustaining the maximum intensity of local electric field. It will be mainly located at the tips of the triangle for a dipolar excitation (left), on the lateral sides for a quadrupolar excitation (center), and slightly on the edges and the apexes at the basis of the triangle for the sextupolar excitation (right).

2 Results and discussion

Gold nanotriangle arrays were fabricated by electron beam lithography in order to control precisely their LSP wavelengths.[37,38] An SEM image of such structures, referred as array A, is shown in the Fig. 2a. It corresponds to a square array of gold equilateral triangles, with edge lengths of 170 nm, a thickness of 50 nm, and an interparticle distance of 340 nm (grating constant, center to center). The experimental optical response of the array revealed two distinctive LSP bands (Fig. 2b, spectrum A): a dominant one at 822 nm, identified as the dipolar LSP mode (1st order), and a less intense one at 614 nm, attributed to the quadrupolar LSP mode (2nd order). The lower intensity observed in the case of the quadrupolar mode, compared to the dipolar one, is due to the specific distribution of oscillating charges limiting a re-radiation in the far-field optical response. The experimental extinction spectrum was compared to the calculated extinction cross section using the FDTD method (Fig. 2b, spectrum B), highlighting a good qualitative agreement between the experimental and theoretical far-field optical response.

The plasmon-induced grafting of aryl layers derived from diazonium salts was performed by simply immersing the nanostructures in a diazonium salt aqueous solution (3 mM), and irradiating the sample during 10 seconds using the appropriate laser. The 785 nm laser line was used to excite the dipolar mode, with maximum extinction resonance located at 822 nm, while the quadrupolar mode at 614 nm was excited using the 633 nm laser line. The optical exposure was performed in normal incidence, and the laser was focused on the array through an immersion microscope objective (100× numerical aperture N.A. 1), resulting in a circular laser spot of 3 μm diameter at the surface.
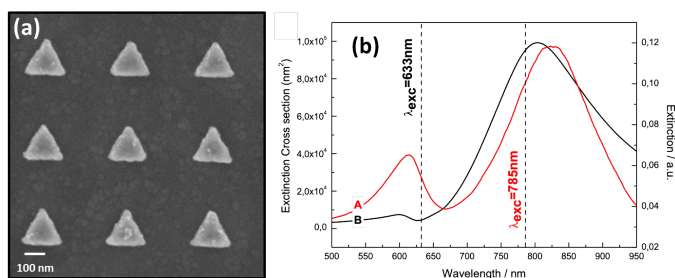
Fig. 2 (a) SEM image of lithographic gold equilateral nanotriangles (170 nm side length, height 50 nm, grating contant 340 nm) over a glass substrate covered by a thin layer of ITO; (b) Far-field optical response (in water): experimental extinction spectrum (spectrum A); extinction cross section calculated by the FDTD method (spectrum B). The laser lines are indicated as vertical dashed lines (at 633 and 785 nm).

Fig. 3 (a) SEM image of the triangles (array A: 170 nm side length, height 50 nm, and grating constant 340 nm), after immersion in an aqueous solution of diazonium salt (3 mM) and optical exposure at 785 nm for a polarization along the X axis; (b) mapping of the intensity of the electric field at 803 nm for a polarization along the X axis, calculated by the FDTD method for a triangular target with 170 nm side length, height 50 nm (bar scale: 50nm); (c) SEM image of the same array of triangles after an optical exposure at 785 nm for a polarization along the Y axis; (d) FDTD mapping of the intensity of the electric field at 803 nm or a polarization along the Y axis (bar scale: 50nm).

Light polarization was tailored in order to be along the base of the triangles (X-polarization), or perpendicular (Y-polarization). After the optical exposure, the grafting was characterized using scanning electron microscopy (SEM), and surface-enhanced Raman spectroscopy (SERS).[39] Fig. 3(a) and Fig. 3(c) display the SEM images of the particles after an exposure of 10 sec. with the 785 nm laser and a polarization along the X- axis and Y- axis, respectively. The laser power was set at 0.13 mW/μm^2, corresponding to an energy dose, defined as the product of the laser power by the optical exposure time, of 1.3 mJ/μm^2. Remarkably, independently of the incident polarization, the SEM images clearly show a nano-localized grafting of organic layers. For the X-polarization, the organic spots are observed mainly at the two apexes of the base of the triangles with identical spatial extent on both sides. In contrast, for the Y-polarization, the grafted layers appear mostly at the top of the triangles. It is noteworthy that the grafting is uniform over the whole sample, as shown in the Fig. SI 1 displaying a SEM image containing more triangles, than the ones showed in Fig. 3(c). Although the mechanism of grafting is still in debate in the literature, it has been shown theoretically that the probability of chemical reactions (such as bonding, or chemical reduction,...) is maximum precisely where there is a maximum of electric field enhancement.[18] A thermal process alone is excluded since it would have had the effect of depositing the organic layer over the entire surface of the particle. The chemical nature of these organic patches has been characterized by SERS, confirming the presence of polyaryl layers derived from nitrobenzene diazonium salts, as shown in the SI (Fig. SI 2a). In addition, after each aryl film grafting, we systematically observed a red-shift of the LSP band, attributed to the increase of the refractive index of the surrounding medium due to the presence of the aryl film (see Fig. SI 2b).

In order to interpret these results, the local electric field distribution was calculated by the FDTD method, with an incident illumination at 803 nm corresponding to the maximum of the dipolar LSP band). The mapping of the local electric field intensity displays maxima situated mainly at the apexes of the structures, with a location depending on the incident polarization. For a polarization parallel to the base of the triangle (X-polarization), the two maxima are located at the apexes located on the base
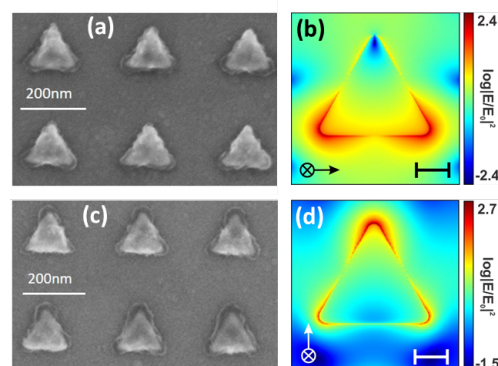
(Fig. 3b). For a perpendicular polarization (Y-polarization), one maximum appears on the apex on the top of the triangle and two other enhanced electric field regions are observed on the base apexes (Fig. 3d). The comparison between the spatial extent of the grafted layers observed by SEM (Fig. 3a and Fig. 3c) and the mapping of the calculated electric field intensity around the triangles (Fig. 3b and Fig. 3d) emphasizes that the distribution of the polyaryl patches is a clear replica of the dipolar near-field intensity.

The quadrupolar mode could also be used to trigger the nano-localized grafting of polyaryl layers derived from diazonium salts, in different nanoscale area. Fig. 4a displays the SEM image of the triangles after an exposure time of 120 sec. with the 633 nm laser line, an incident Y-polarization, and a laser power of 0.06 mW/μm^2. It shows that the aryl patch distribution is radically different from that observed under excitation of the dipolar mode at 785 nm (Fig. 3), with organic layers mainly observed at the three edges of the triangles. As evidenced in Fig. 4b, the spatial extent of the grafting nicely follows the mapping of the electric field intensity using the FDTD method, for an incident illumination at 600 nm, related to the excitation of the quadrupolar LSP mode. It is worth noting that both X- and Y-polarization of incident light result here in comparable patterns (Fig. 4a and Fig. 4c) due to the similarity of the electric field intensity distribution of these configurations (Fig. 4b and Fig. 4d). In contrast to the dipolar mode, the choice of the incident polarization (X- or Y-polarization) for the quadrupolar mode does not change significantly the location of the aryl film.

In order to confirm that the location of the plasmon-induced grafting is not governed by the excitation line, but rather by the excitation of the distinct LSP modes, two new arrays of triangles were designed. The first one (array B) with a dipolar LSP mode matching the laser line at 633 nm, is made of equilateral triangles, with edge lengths of 90 nm, a thickness of 50 nm, and a
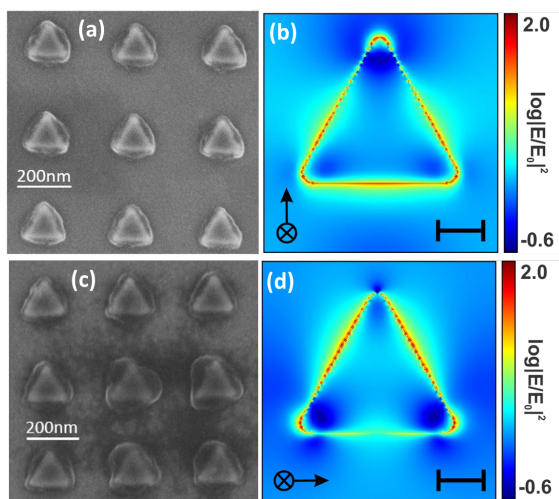
Fig. 4 (a) SEM image of the triangles (array A), after immersion in an aqueous solution of diazonium salt (3 mM) and optical exposure at 633 nm for a polarization along the Y axis; (b) mapping of the intensity of the incident electric field at 600 nm, calculated by the FDTD method for a triangular target with 170 nm side length, height 50 nm, and a grating constant of 340 nm (polarization along the Y axis); (c) SEM image of the triangles, after optical exposure at 633 nm for a polarization along the X axis; (d) FDTD mapping of the intensity of the incident electric field at 600 nm, for the same triangular target (polarization along the X axis) - bar scale: 50 nm.

Fig. 5 (a) Experimental extinction spectrum of equilateral triangles: spectrum A, with edge lengths of 170 nm, a thickness of 50 nm, and grating constant of of 340 nm (in inset, SEM image of a single triangle), and spectrum B, with edge lengths of 90 nm, a thickness of 50 nm, and grating constant of of 400 nm (in inset, SEM image of a single triangle). The spectrum is recorded in water; (b) FDTD mapping of the intensity of the electric field at 690 nm, and a polarization along the Y axis for the triangle of 90 nm edge; (c) SEM image of a 90 nm edge triangle, after immersion in an aqueous solution of diazonium salt (3 mM) and optical exposure at 633 nm for a polarization along the Y axis.

grating constant of 400 nm (see inset of Fig. 5a). As a result, a single LSP band is emerging at 668 nm in the extinction spectrum recorded in water, associated with the dipolar mode (see Fig. 5a, spectrum B). This is in accordance with the FDTD calculations, showing a single extinction cross section band at 690 nm, and a mapping of the electric field associated with a dipolar character (Fig. 5b, and Fig. SI3). It is thus expected that, for a laser line at 633 nm, the excitation of the dipolar mode induces an aryl film grafting at the apexes of the triangles, and not at the edges. The experimental results obtained after an exposure time of 60 sec. at 633 nm, with an energy dose of 0.5 mJ/μm^2 and a polarization along the Y-axis, confirm this hypothesis, with polyaryl patches appearing exclusively at the apexes of the triangles (Fig. 5c). For the array A (spectrum A), an excitation at 633 nm, upon excitation of its quadrupolar mode, leads to a site-selective organic coating located at the edges, and not at the apexes (Fig. 4a and Fig. 4b).

We considered an additional array (array C), displaying a quadrupolar mode close to 785 nm. This array C was made of equilateral triangles, with edge lengths of 250 nm, a thickness of 40 nm, and a grating constant of 400 nm (Fig. 6a, inset). As a result, a LSP band is emerging (in water) at 740 nm in the extinction spectrum, attributed to the quadrupolar mode (Fig. 6a). For a density of energy of 9 mJ/μm^2 at 785 nm, and a polarization along the Y-axis, the aryl film grafting is located at the edges of the triangles, in agreement with the excitation of the quadrupolar mode (Fig. 6b). The location of the grafting nicely follows the mapping of the electric field intensity associated to the quadrupolar mode calculated at 725 nm (Fig. 6c), and can be compared to the mapping of array A, for which the grafting, at 785 nm, fol-
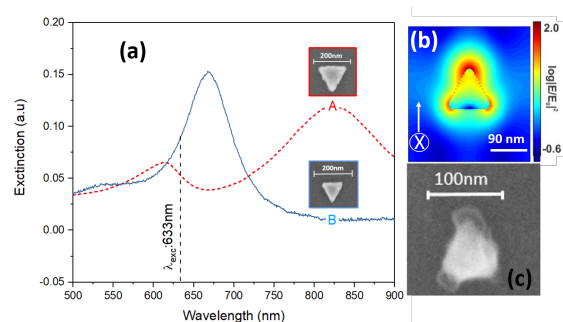
lows the mapping of the dipolar mode (Fig. 3). It can thus be concluded that the location of the aryl film grafting is only governed by the order of the chosen multipolar mode, and not by the laser line.

Interestingly, the array C displays an additional LSP band located at 590 nm, attributed to the 3rd order of the LSP mode, the so-called sextupolar mode. The mapping of the associated calculated electric field reveals a slightly distinct electric field distribution (calculated at 610 nm), compared to the dipolar and quadrupolar ones, with an assymetric distribution of the electric field along the lateral edges, and two maxima at the apexes of the triangle base (Fig. 6e). To investigate the possibility to induce site-selective surface grafting of aryl layers under excitation of this sextupolar mode, array C was immersed in the diazonium salt solution and exposed to irradiation at 633 nm, close to the wavelength of the sextupolar mode. With a density of energy of 7 mJ/μm^2 and a polarization along the Y-axis, yielded a distinctive pattern with a maximum grafting at the apexes of the triangles, and an asymmetric distribution along the edges (Fig. 6d and 6e). The location of the grafting thus qualitatively follows the mapping of the electric field associated to the sextupolar mode.

Some differences have to be pointed out between the location of the aryl film grafting and the electric field mapping for the sextupolar mode (Fig. 6d and Fig. 6e). The grafting along the edges is not as obvious, in comparison with the mapping of the electric field, although it slightly appears at the top of the two edges. However, the two other grafting locations are clearly observed at the two apexes of the base of the triangles, in good qualitative agreement from the FDTD calculations. Despite the poor matching conditions of the excitations wavelengths, these pre-resonances conditions appear effective to photoinduce the onset of spatially controlled polymerization that mimic the FDTD mapping calculated at the resonances. This is clearly shown in 6b and Fig. 6c for the quadrupolar mode and for 6d and Fig. 6e for the sextupolar mode. Better matching conditions would presumably
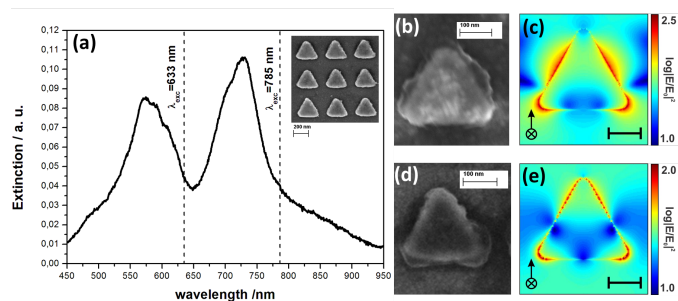
Fig. 6 (a) Experimental extinction spectrum in water of gold nanotriangles (array C): lateral size: 250 nm, height: 40 nm, grating constant: 400 nm. Inset: SEM image of the corresponding triangles; (b) SEM image of a triangle, after immersion in an aqueous solution of diazonium salt (3 mM) and optical exposure at 785 nm for a polarization along the Y axis (exposure conditions: 9 mJ/μm^2). (c): mapping of electric field intensity at 725 nm irradiation, calculated by the FDTD method. Scale bar: 50 nm; (d): SEM image of a triangle, after optical exposure at 633 nm for a polarization along the Y axis (exposure conditions: 7 mJ/μm^2); (e): mapping of electric field intensity at 610 nm irradiation, calculated by the FDTD method. Scale bar: 50 nm.

yield more effective spatial localization with shorter irradiation or lower irrandiance. It can be also noted that the grafting, through the sextupolar mode, leads to a pattern similar to the one obtained for a dipolar mode. This similarity precisely points out the versatility of our strategy: being able to position the organic layer at any locations, regardless the size of the triangles.

One critical aspect deals with the control of the thickness of the aryl film layer, which is of main importance in the context of biosensing applications or surface-enhanced spectroscopy analyses to adjust the distance between the particle surface and the probed analytes.[40] In order to tune the organic patch thickness and spatial extent, the energy dose was varied, from 0.69 to 8.3 mJ/μm^2. The SEM images of array A, after quadrupolar mode-induced grafting (at 633 nm) and a dipolar mode illumination (at 785 nm) respectively, are displayed in Fig. 7a at increasing energy doses. An average thickness was measured as the distance between the particle surface and the upper end of the thicker area of the aryl film layers versus the energy dose for both modes. From these SEM images, it appears that the thickness of the grafted organic layers increases progressively with the energy dose, inducing a higher degree of polymerization, while remaining strongly confined in intense electric field area. As reported in Fig. 7b, the average film thickness reaches *ca.* 50-60 nm at high energy dose (8.3 mJ/μm^2) with a tendency to plateau, at least for the dipolar mode. This plateau is attributed to the fact that the near-field enhancement is maximum at the particle surface, but decreases rapidly exponentially with the distance from the surface.[26] Interestingly, it can be noted that for a given incident energy dose, the layer thickness is systematically higher for a dipolar excitation, compared to the quadrupolar one. This trend can be attributed to the fact that the intensity of the dipolar electric field is higher than the intensity of the quadrupolar one, for a given intensity of the incident electric field.[6] The thickness of the polyaryl film can thus be controlled by both the energy dose and

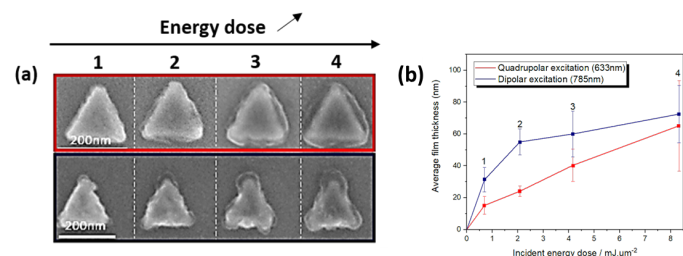the selected multipolar LSP mode.

Fig. 7 (a) SEM images of the array A after immersion in aqueous diazonium salt solution (3 mM), and optical exposure at various energy doses ranging from (1) 0.69 mJ/μm^2, (2) 2.08 mJ/μm^2 (3) 4.1 mJ/μm^2 to (4) 8.3 mJ/μm^2 Exposures were made at 633 nm, corresponding to the excitation of the quadrupolar mode (top frame surrounded in red), and at 785 nm, corresponding to the excitation of the dipolar mode (bottom frame surrounded in blue); (b) Average thickness, measured as the distance between the particle surface and the upper end of the thicker area of the aryl film layers versus the energy dose for the dipolar (blue squares) and quadrupolar (red squares) LSP modes.

3 Conclusion

In summary, we have shown that the excitation of multipolar LSP modes expands the possibilities of plasmon-driven surface functionalization with aryl diazonium salts and opening new routes of surface chemistry and patterning. By playing on various multipolar modes, different chemical patterns could be accessible, from the nano-localized grafting of organic patches exclusively on the apexes of triangular NPs upon dipolar mode excitation, to the confinement of organic layers specifically on the edges by illuminating the quadrupolar mode. Interestingly, the sextupolar mode could also be used to trigger a different chemical pattern. By systematically comparing the experimental results with the mapping of the electric field intensity calculated by the FDTD method, it appears that the multipolar plasmon-induced grafting occurs specifically in the regions of maximum field enhancement, leaving the other areas of the nanostructure's surface chemically passive. In addition, the thickness of the organic patches can be tailored by changing the energy dose and the selected LSP mode, from few nm up to 50-60 nm, opening promising prospects for nanosensing.

4 Experimental section

Gold nanotriangle arrays were fabricated by electron beam lithography in order to achieve a precise monitoring of their LSP wavelengths, and to ensure that the LSP modes match well with the available excitation lines at 633 nm (He-Ne laser), and 785 nm (Laser diode). For their fabrication, a 190 nm thick layer of poly(methyl methacrylate) (PMMA) electron resist was spin coated on glass substrates covered with a 80 nm layer of transparent conducting indium tin oxide (ITO). In the exposure step, the substrates were exposed to an electron beam which was scanned over the sample. Chemical development, thermal vacuum coating with gold and a lift-off procedure followed, which led to regular arrays of gold triangular structures exhibiting 35-50 nm height and variable edge lengths and inter-particle distances (grating

constant, center to center).

The diazonium salt which was used to induce the plasmon-mediated grafting of aryl films is 4- nitrobenzenediazonium tetrafluoroborate (4NBDT). The plasmon-induced grafting of aryl layers derived from diazonium salts was performed by simply immersing the nanostructures in a diazonium salt aqueous solution (3 mM), and irradiating the sample at various times using the a 633 or 785 nm laser lines. The optical exposure was performed in normal incidence, and the laser was focused on the array through an immersion microscope objective (100× numerical aperture N.A. 1), resulting in a circular laser spot of 3 μm diameter at the surface.

The LSP resonance of the samples was probed by far-field visible-NIR extinction micro-spectroscopy in the range of 500–900 nm, with irradiation by using a halogen lamp at normal incidence from the glass side. The spectrometer was coupled to an optical microscope equipped with a 50× objective (numerical aperture N.A.0.75). The investigated area was a circle of approximately 80 μm diameter, which was covering the entire array (100×100 μm^2). The spectra were recorded in water, since the LSP-induced grafting of the diazonium salt takes place in this medium.

The Raman and SERS experiments were carried out by using a Jobin-Yvon LABRAM HR 800 Raman micro spectrometer. The incident sources are a He–Ne laser (632.8 nm), and a laser diode (785 nm) focused on the sample, through a microscope equipped with a 100× objective (Olympus, NA 0.8).

Finite-difference time-domain (FDTD) modelling (Lumerical FDTD Solutions) was used to simulate the extinction cross-section and the electric field at the surface of the triangular nanoparticles. The gold triangular nanoparticles were of size and thickness as indicated. The structures were modelled on a substrate of refractive index 1.78 to match the ITO substrate,[41] and the surrounding medium of refractive index of 1.33 to match the surrounding water.[42] The gold was modelled using the dielectric functions of gold from Palik.[43] To match the array fabricated experimentally, periodic boundary conditions were set along the X- and Y-boundaries, set to match the grating constant of the array. In order to truncate the simulation area, perfectly matched layers were applied along the Z-boundary. The structures were meshed by a grid of 2 nm in the X-, Y- and Z-directions. A maximum of 10 mesh cells per wavelength was applied outside of the triangular nanoparticles.

Conflicts of interest

There are no conflicts to declare.

Acknowledgements

Notes and references

1 M. Pelton, J. Aizpurua and G. Bryant, *Laser & Photonics Reviews*, 2008, **2**, 136–159.
2 J. A. Creighton and D. G. Eadon, *Journal of the Chemical Society, Faraday Transactions*, 1991, **87**, 3881–3891.
3 V. G. Kravets, A. V. Kabashin, W. L. Barnes and A. N. Grigorenko, *Chemical Reviews*, 2018, **118**, 5912–5951.
4 R. Hong, W. Shao, W. Sun, C. Deng, C. Tao and D. Zhang, *Optical Materials*, 2018, **83**, 212–219.
5 S. A. Maier, *Plasmonics: fundamentals and applications*, Springer Science & Business Media, 2007.
6 E. Hao and G. C. Schatz, *The Journal of chemical physics*, 2004, **120**, 357–366.
7 A. Trügler, J.-C. Tinguely, G. Jakopic, U. Hohenester, J. R. Krenn and A. Hohenau, *Physical Review B*, 2014, **89**, 165409.
8 J. Butet, P.-F. Brevet and O. J. Martin, *ACS nano*, 2015, **9**, 10545–10562.
9 X. Wu, C. Hao, J. Kumar, H. Kuang, N. A. Kotov, L. M. Liz-Marzán and C. Xu, *Chem. Soc. Rev.*, 2018, **47**, 4677–4696.
10 J. Zhou, T. Yang, J. Chen, C. Wang, H. Zhang and Y. Shao, *Coordination Chemistry Reviews*, 2020, **410**, 213218.
11 I. Haidar, G. Lévi, L. Mouton, J. Aubard, J. Grand, S. Lau-Truong, D. R. Neuville, N. Félidj and L. Boubekeur-Lecaque, *Physical Chemistry Chemical Physics*, 2016, **18**, 32272–32280.
12 C. Matricardi, C. Hanske, J. L. Garcia-Pomar, J. Langer, A. Mihi and L. M. Liz-Marzan, *ACS Nano*, 2018, **12**, 8531–8539.
13 E. Kazuma and Y. Kim, *Angewandte Chemie International Edition*, 2019, **58**, 4800–4808.
14 G. Baffou and R. Quidant, *Chemical Society Reviews*, 2014, **43**, 3898–3907.
15 C. Boerigter, U. Aslam and S. Linic, *ACS nano*, 2016, **10**, 6108–6115.
16 E. Miliutina, O. Guselnikova, N. S. Soldatova, P. Bainova, R. Elashnikov, P. Fitl, T. Kurten, M. S. Yusubov, V. Svorcik, R. R. Valiev *et al.*, *The Journal of Physical Chemistry Letters*, 2020, **11**, 5770–5776.
17 A. Olshtrem, O. Guselnikova, P. Postnikov, A. Trelin, M. Yusubov, Y. Kalachyova, L. Lapcak, M. Cieslar, P. Ulbrich, V. Svorcik *et al.*, *Nanoscale*, 2020, **12**, 14581–14588.
18 N. H. Kim, C. D. Meinhart and M. Moskovits, *The Journal of Physical Chemistry C*, 2016, **120**, 6750–6755.
19 Y. Kim, J. G. Smith and P. K. Jain, *Nature Chemistry*, 2018, **10**, 763–769.
20 C. Lu, J. Li, J. Yan, B. Li, B. Huang and Z. Lou, *Applied Materials Today*, 2020, **20**, 100744.
21 B. B. Rajeeva, D. S. Hernandez, M. Wang, E. Perillo, L. Lin, L. Scarabelli, B. Pingali, L. M. Liz-Marzán, A. K. Dunn, J. B. Shear *et al.*, *Advanced Science*, 2015, **2**, 1500232.
22 M. Nguyen, A. Lamouri, C. Salameh, G. Lévi, J. Grand, L. Boubekeur-Lecaque, C. Mangeney and N. Félidj, *Nanoscale*, 2016, **8**, 8633–8640.
23 J. Pinson and F. Podvorica, *Chem. Soc. Rev.*, 2005, **34**, 429–439.
24 Y. Luo, Y. Xiao, D. Onidas, L. Iannazzo, M. Etheve-Quelquejeu, A. Lamouri, N. Félidj, S. Mahouche, T. Brulé, N. Eilstein *et al.*, *Chemical Communications*, 2020.
25 D. A. Therien, N. M. Ćulum, D. M. McRae, L. Mazaheri and F. Lagugné-Labarthet, *Optical Materials*, 2021, **112**, 110775.
26 I. Tijunelyte, I. Kherbouche, S. Gam-Derouich, M. Nguyen, N. Lidgi-Guigui, M. L. de la Chapelle, A. Lamouri, G. Lévi, J. Aubard, A. Chevillot-Biraud *et al.*, *Nanoscale Horizons*, 2018, **3**, 53–57.
27 M. Nguyen, I. Kherbouche, S. Gam-Derouich, I. Ragheb, S. Lau-Truong, A. Lamouri, G. Lévi, J. Aubard, P. Decorse, N. Félidj *et al.*, *Chemical Communications*, 2017, **53**, 11364–11367.
28 V.-Q. Nguyen, Y. Ai, P. Martin and J.-C. Lacroix, *ACS omega*, 2017, **2**, 1947–1955.
29 G. Q. Wallace, M. Tabatabaei, R. Hou, M. J. Coady, P. R. Norton, T. S. Simpson, S. M. Rosendahl, A. Merlen and F. Lagugné-Labarthet, *ACS Photonics*, 2016, **3**, 1723–1732.
30 M. Tabatabaei, A. Sangar, N. Kazemi-Zanjani, P. Torchio, A. Merlen and F. Lagugné-Labarthet, *The Journal of Physical Chemistry C*, 2013, **117**, 14778–14786.
31 R. Marty, G. Baffou, A. Arbouet, C. Girard and R. Quidant, *Optics Express*, 2010, **18**, 3035–3044.
32 I. C. Bicket, E. P. Bellido, D. M. McRae, F. Lagugné-Labarthet and G. A. Botton, *ACS Photonics*, 2020, **7**, 1246–1254.
33 N. Felidj, J. Grand, G. Laurent, J. Aubard, G. Levi, A. Hohenau, N. Galler, F. Aussenegg and J. Krenn, *The Journal of chemical physics*, 2008, **128**, 094702.
34 D. Belanger and J. Pinson, *Chemical Society Reviews*, 2011, **40**, 3995–4048.
35 T. G. Jurgens and A. Taflove, *IEEE Transactions on Antennas and Propagation*, 1993, **41**, 1703–1708.
36 L. Guerrini, Ž. Krpetić, D. van Lierop, R. A. Alvarez-Puebla and D. Graham, *Angewandte Chemie*, 2015, **127**, 1160–1164.
37 W. Gotschy, K. Vonmetz, A. Leitner and F. Aussenegg, *Applied Physics B*, 1996, **63**, 381–384.
38 N. Félidj, G. Laurent, J. Grand, J. Aubard, G. Lévi, A. Hohenau, F. R. Aussenegg and J. R. Krenn, *Plasmonics*, 2006, **1**, 35–39.
39 I. Haidar, A. Day, U. Martino, A. Chevillot-Biraud, N. Félidj and L. Boubekeur-Lecaque, *Applied Materials Today*, 2019, **15**, 462–471.
40 M. Nguyen, I. Kherbouche, M. Braik, A. Belkhir, L. Boubekeur-Lecaque, J. Aubard, C. Mangeney and N. Felidj, *ACS omega*, 2019, **4**, 1144–1150.
41 T. A. Konig, P. A. Ledin, J. Kerszulis, M. A. Mahmoud, M. A. El-Sayed, J. R. Reynolds and V. V. Tsukruk, *ACS nano*, 2014, **8**, 6182–6192.
42 G. M. Hale and M. R. Querry, *Applied optics*, 1973, **12**, 555–563.
43 E. D. Palik, *Handbook of optical constants of solids*, Academic press, 1998, vol. 3.